© creative

Scientific paper

Synthesis of Bone Meal-derived 4-Carboxyphenylboronic Acid Functionalized Sulfur and Nitrogen Co-doped Graphene Quantum Dots Nanoprobe for Sialic Acid Sensing

Sopan N. Nangare,^{1#} Pratik P. Yeole,^{1#} Zamir G. Khan,¹ Ashwini G. Patil,¹ Bhushankumar S. Sathe,² Sanjaykumar B. Bari¹ and Pravin O. Patil^{1,*}

¹ Department of Pharmaceutical Chemistry, H. R. Patel Institute of Pharmaceutical Education and Research, Shirpur-425405, Dist: Dhule (MS); India

² VYWS Institute of Diploma in Pharmacy, Borgaon, Wardha (MS)- 442001; India

* Corresponding author: E-mail: rxpatilpravin@yahoo.co.in

Received: 08-09-2023

These authors contributed equally as the first authors.

Abstract

Detection of sialic acid using advanced sensors in milk-based products is essential in the food industry. Therefore, the present work reports the sulfur and nitrogen-doped graphene quantum dots from bone meal functionalized with boronic acid (Boro-S/N-dGQDs) nanoprobe for sialic acid sensing applications. Briefly, S/N-dGQDs were functionalized with 4-carboxyphenylboronic acid to improve performance of fluorescent sensors toward the detection of sialic acid. Here, boronic acid surface decoration on S/N-dGQD was confirmed by several spectral characterizations. The addition of different quantities of sialic acid results in a directly proportionate correlation to fluorescence quenching. It gives a broad linear range of 50 ng/mL to 1000 ng/mL and a limit of detection of 6.04 ng/mL. Also, it displayed remarkable selectivity, likely due to interaction of sialic acid-containing 1,2-diol with hydroxyl group of Boro-S/N-dGQDs nanoprobe. Designed sensor demonstrated good stability and reproducibility. Real-time analysis of sialic acid in different milk-based products confirmed practicability of Boro-S/N-dGQDs.

Keywords: Bone meal; Boro-S/N-dGQDs; boronic acid; sialic acid; milk products; fluorescent sensor

1. Introduction

Sialic acid is a negatively charged monosaccharide that is present at the ends of glycolipids and glycoproteins on the cell surface. In addition, sialic acid is present in milk, meat, and other foods.² According to the literature, sialic acid is present in mammalian glycoconjugates. Here, the hydroxylated form of sialic acid is absent in humans. On the contrary, sialic acid is present in mammals. Therefore, the consumption of milk-based products and meat with high concentrations of a hydroxylated form of sialic acid (non-human sialic acid) can pose health risks.³ Here, the chronic consumption of the hydroxylated form of sialic acid can result in chronic inflammation, leading to different types of diet-associated cancers, as well as other types of health issues. 4,5 Therefore, there is a need to monitor the level of the hydroxylated form of sialic acid in milk products.

To date, several techniques for detecting sialic acid have been recorded. In brief, electrochemical methods such as potentiometric, non-enzymatic electrochemical, organic electrochemical transistors, electrochemical impedance spectroscopy, etc. have been documented for the detection of sialic acid. Other methods for the detection of sialic acid include chromatography, colorimetry, and spectrofluorimetry. Despite their several advantages, there are some disadvantages, such as the usage of harmful and expensive chemicals in the sensor's construction, limited selectivity, poor sensitivity, time-consuming, complex processing, and so on. Therefore, there is a pressing urgency to produce a highly sensitive, green-made, simple, highly selective, cost-effective, quick sensor for sialic acid identification in milk-based products.

The adoption of a fluorescence-based sensor overcomes various demerits of the previously utilized approach

for the identification of interest compounds. 10 In the case of fluorescence-based sensors, the scientific community has established a strong preference for carbon-mediated zero-dimensional nanosized fluorescent particles known as graphene quantum dots (GQDs) for a variety of applications. The nanosize design of GQDs is a crystalline graphitic material founded on sp²-hybridized carbon.¹¹ Furthermore, owing to their edge effects and strong quantum confinement, GQDs have excellent stability, minute toxicity, and good fluorescence. 12 As well, it has strong biocompatibility, great solubility, an adjustable band gap, and others.¹³ During the last few decades, GODs have been modified for sensing applications employing several types of heteroatoms.¹⁴ According to the literature, heteroatom-doped GQDs may efficiently modify their chemical and physical properties. 13 In this shade, GQD doping allows for changes in energy density, band gap, and other properties. 12

As explained, heteroatom doping in GQDs raised the aggregate capability of fluorescence-based sensors for extremely sensitive and selective analyte recognition. ^{15,16} For the design of heteroatom-doped GQDs, the preference for green precursor has been reported ¹⁷ to avoid exposure to chemicals followed by toxicity. ¹⁰ Moreover, the use of biomass such as honey, orange juice, green tea extract, rice husk, etc. for the design of GQDs ¹⁸ provides several advantages including abundant surface functionality, high carbon composition, cost-effectiveness, eco-friendly, etc. ¹⁰ Finally, the green-made doped GQDs showcased upgraded sensor performance. ^{10,17} As a result, we prefer to develop green-made doped GQDs for sialic acid sensing applications.

Of particular importance, nitrogen (N) and sulfur (S) are the most widely employed doping agents for the production of doped GQDs. 17,19 Because of their five valence electrons and equivalent atomic size, 'N' doping is capable of bonding with the carbon backbone of GQDs. According to the literature, the design of 'N' doping in a GQD lattice can drastically affect the electrical and chemical characteristics, as well as impart a large number of sites for additional adjustments. 13 Likewise, the preference for 'S' doping in GQDs has been reported.²⁰ In this case, the doping of S' can aid in improving the electron transfer process.²¹ On this basis, the design of 'S' and 'N' doped GQDs (S/N-dGQDs) have been majorly documented for plentiful sensing²² and other applications.²¹ Despite the considerable degree of customization in GQDs utilizing various dopants, high sensitivity, and selectivity are critical tasks in sensing applications.²³ In recent years, the functionalization of fluorescent nanoparticles such as GQDs has been described as offering an improved presentation for the detection of interest analytes.²⁴ In short, greenmade GQDs with appropriate functionalizing agents have been described for sensing applications^{25,26} that furnish advanced sensing performance. In this light, the selectivity for the analyte of interest in the involvement of various interfering agents has been explained as acceptable for functionalizing agents.^{23,25,26} More importantly, the design of surface functionalized S/N-dGQDs for sialic acid sensing in milk-based products has yet to be released. As a result, the synergistic benefits of surface functionalized S/N-dGQDs may grant increased sensitivity and selectivity than the previously published techniques.

Therefore, the current study presents a simplistic, highly sensitive, highly selective, green-made, and stable Boro-S/N-dGQDs-based fluorescence sensor for sialic acid detection in milk products. In summary, the hydrothermal approach was adopted to achieve a green synthesis of S/N-dGQDs as a fluorescent agent, with bone meal serving as both a green precursor and a dopant source. Subsequently, the generated S/N-dGQDs were functionalized with boronic acid, and fluorescence analysis confirmed enhanced fluorescence compared to the S/NdGQDs. FT-IR, PXRD, HR-TEM, XPS, Raman, zeta potential, fluorescence research, and other techniques were employed to verify the successful synthesis of S/NdGQDs and Boro-S/N-dGQDs. The sialic acid sensing using Boro-S/N-dGQDs exhibited a proportional connection to fluorescence quenching. It demonstrated a wide linear concentration range and a detection limit of 50 ng/ mL for sialic acid. Moreover, it displayed significant anti-interference potential, attributed to the interaction of sialic acid-containing 1,2-diol with a hydroxyl group of Boro-S/N-dGQDs. Consequently, the study confirmed the synergistic effect of dopants and functionalizing agents used in GQDs to enhance fluorescence sensor performance for sialic acid detection, surpassing previously reported approaches. At last, the different local milk products were analyzed confirming the real-time applications of the proposed sensor for the detection of sialic acid. Overall, Boro-S/N-dGQDs offer several advantages, including enhanced sensitivity, excellent selectivity, superior stability, eco-friendliness, cost-effectiveness, simplicity, and more, which will pave the way for future monitoring safety of milk-based products.

2. Materials and Methods

2. 1. Materials

The bone meal was collected from the local market in Shirpur, Maharashtra, India. Sialic acid ($C_{11}H_{19}NO_9$, N-acetylneuraminic acid, Mol. Wt: 309.27 g/mol] was purchased from Tokyo Chemical Industry Co. Ltd. Chennai, Tamil Nadu, India. 4-carboxyphenylboronic acid ($C_7H_7BO_4$; 4-CPBA; Mol. Wt: 165.94 g/mol] was purchased from Tokyo Chemical Industry Co. Ltd. Chennai, Tamil Nadu, India. The citric acid ($C_6H_8O_7$; 2-hydroxypropane-1,2,3-tricarboxylic acid; Mol. Wt: 192.12 g/mol], sodium chloride (NaCl), uric acid, ferric chloride (FeCl₃), magnesium sulfate (MgSO₄), and potassium chloride (KCl), etc. were purchased from Loba Chemie Pvt. Ltd. Mumbai, India. Double

distilled water (DDW) was purchased from Ranchem Pvt. Ltd. India. For this research work, all chemicals and reagents were utilized exactly as they were obtained.

2. 2. Methods

2. 2. 1. Synthesis of Bare GQDs

In this work, the synthesis of bare GQDs was performed utilizing a previously published method. In brief, 2 g citric acid was added to 30 mL of DDW. After that, the resulting solution underwent a hydrothermal procedure in a stainless steel autoclave coated with Teflon. In this case, the temperature of the operation was sustained at 160 °C for 8 h in a programmed hot air oven (Bio-Technics India)¹⁶. Following the completion of the hydrothermal procedure, the yellow-colored GQDs solution was filtered using 0.22 µm membrane filter paper. Herein, cold centrifugation was used to concentrate the filtrate at 14000 rpm for 45 min at 20 °C. After this, a freeze-drying procedure was used to finish the drying. Finally, bare GQDs were employed to validate fluorescence amplification following doping and functionalization of GQDs.

2. 2. 2. Green Synthesis of S/N-dGQDs

In this step, the green synthesis of S/N-dGQDs was completed from bone meal. In brief, bone meal (1 g) was blended in a glass beaker carrying 50 mL of DDW. Following this, the produced dispersion was exposed to a single-step hydrothermal procedure in a stainless steel autoclave lined with Teflon. The hydrothermal procedure was carried out for 9 h at 160 °C in a laboratory vacuum oven. 16 In this part of the process, the initially produced dispersion of bone meal was altered to a dark brown color. Next, filtration was performed on the treated dispersion using 0.22 μ m membrane filter paper. Then, the filtrate was concentrated using cold centrifugation at 14000 rpm for 45 min at 20 °C. Last, the freeze-drying method was employed to dry up the produced S/N-dGQDs. 27

2. 2. 3. Synthesis of Boro-S/N-dGQDs

In this step, the synthesis of fluorescent Boro-S/N -dGQDs was accomplished (Scheme 1) for the detection of sialic acid. In short, 4 mL of S/N-dGQDs (100 ng/mL) and phosphate-buffered solution (PBS, pH 7.4) were appropri-



Scheme 1: Synthesis of Boro-S/N-dGQDs from bone meal-derived S/N-dGQDs from bone meal powder

ately mixed (1:1). After that, the solution was treated with 24 mg of 4-CPBA to form Boro-S/N -dGQDs. Here, the resulting mixture was incubated at room temperature for 3 h with constant stirring at 100 rpm. Followed by, the obtained Boro-S/N-dGQDs were filtered using a membrane filter whereas the filtrate was dialyzed for 48 h against PBS (pH 7.4) in a dialysis bag (Mol Wt. cut-off: 3500 Da) to provide pure Boro-S/N -dGQDs.23 At last, the freeze-drying method was employed to dry the produced Boro-S/N-dGQDs.

2. 2. 4. Characterizations of Bare GQDs, S/N-dGQDs, Boro-S/N-dGQDs

The ultraviolet-visible (UV-Vis) spectrophotometer (UV 1800 Shimadzu, Japan) was chosen to ensure the synthesis of bare GQDs, S/N-dGQDs, and Boro-S/N-dGQDs using a quartz cuvette (width: 1 cm) and a scanning wavelength range of 200 nm to 800 nm. The fluorescence study of bare GQDs, S/N-dGQDs, and Boro-S/N-dGQDs was performed using a UV cabinet (Southern scientific lab instrument, India) and spectrofluorometer spectrophotometer (Jasco, FP-8200, Japan). In addition, the excitation and emission of Boro-S/N-dGQDs were reported using a spectrofluorometer. The excitation wavelength-dependent emission of Boro-S/N-dGQDs was measured by altering the excitation wavelength (range 310 nm - 370 nm) using a spectrofluorometer. The Fourier transform infrared (FT-IR, Bruker, ALPHA II Compact FT-IR Spectrometer) spectrophotometer was used to confirm the functionality present in bare GQDs, S/N-dGQDs, and Boro-S/N-dGQDs. In FT-IR analysis, the samples were scanned from a range of 600 nm to 4000 nm with 22 scans. The particle size, zeta potential, and polydispersity index (PDI) of obtained nanomaterials bare GQDs, S/N-dGQDs, and Boro-S/N -dGQDs were assessed using a particle size analyzer (NanoPlus3, Micromeritics, USA). The crystalline nature of prepared modified nanomaterials was evaluated using a powder X-ray diffractometer (Bruker Kappa Apex II). The elemental composition of bone meal was confirmed using Energy-dispersive X-ray analysis (EDAX, Jeol/OXFORD XMX N). (EDAX) The Raman analysis of S/N-dGQDs and Boro-S/N-dGQDs was completed using via Raman spectroscopy (Renishaw). The X-ray photoelectron spectroscopy (XPS, Physical Electronics, PHI 5000 Versa Probe III) was used to verify the surface functionality of S/N-dGQDs and Boro-S/N-dGQDs. The particle size and morphology of S/N-dGQDs and Boro-S/N-dGQDs were validated using high-resolution-transmission electron microscopy [HR-TEM, Joel/JEM 2100] in which LaB₆ light was preferred as an electron gun.

2. 2. 6. pH-dependent Fluorescence Stability

In this step, the impact of pH on the fluorescence property of Boro-S/N-dGQDs was confirmed. At first, the

Boro-S/N-dGQDs (100 ng/mL) were freshly prepared using DDW as a stock. After this, 5 mL of Boro-S/N-dGQDs was added into a separate test tube for further analysis. Herein, different pH (range from pH 3, 5, 7, 9, and 11) of Boro-S/N-dGQDs was adjusted using 1 M NaOH and 1 M HCl. Afterwards, the solutions were kept for 30 min at below 25 °C temperature. Finally, the impact of pH on the fluorescent property of Boro-S/N-dGQDs was assessed using a spectrofluorometer at $\lambda_{\rm max}$ of 360 nm (excitation wavelength). After this, the UV cabinet was preferred to inspect the change in fluorescence of the Boro-S/N-dGQDs sensor under different lights such as visible light, short wavelength ($\lambda_{\rm max}$ = 254 nm), and long wavelength ($\lambda_{\rm max}$ = 365 nm). As well, pH-based fluorescence correlation was verified via zeta potential analysis.

2. 2. 7. Determination of Percent Quantum Yield (% QY)

In this study, the % of QY of bare GQDs, S/N-dGQDs, and Boro-S/N-dGQDs was calculated using the formerly reported method.26 The '% QY' of bare GQDs, S/N-dGQDs, and Boro-S/N-dGQDs was determined using the following Equation 1,

$$\varphi_x = \varphi_{st} \left(\frac{Grad_x}{Grad_{st}} \right) \left(\frac{\eta_x}{\eta_{st}} \right) \tag{1}$$

In this equation 1, ' φ ' denotes the QY. As well, the subscripts 'x' and 'st' stand for a test and standard, accordingly. The ' η ' denotes the refractive index (RI) of solvents.

2. 2. 8. Sensing of Sialic Acid

At first, Boro-S/N-dGQDs (100 µg/mL) were prepared freshly for sensitivity application. In concisely, 5 mL of prepared Boro-S/N-dGQDs was added into each test tube as a fluorescent sensing probe for the recognition of sialic acid. Then, the selected range of sialic acid concentration from 50 ng/mL to 1000 ng/mL was prepared using pH 7.4 phosphate buffer in a separate sample tube. The first concentration of sialic acid was added into the Boro-S/N-dGQDs and then it was kept aside for 10 min to complete the reaction. After this, the probe was subjected to a fluorescence study to verify the suppression of fluorescence of Boro-S/N-dGQDs. Similarly, different concentrations of sialic acid were added to the probe solution to obtain the linearity. Finally, the relation of concentration of sialic acid vs fluorescence quenching of Boro-S/N-dGQDs was investigated. As well, the limit of detection (LOD) and limit of quantification (LOQ) was assessed using slope and standard deviation. Equation 2 and Equation 3 were used for LOD and LOQ measurements.28

$$LOD = 3.3 \left(\frac{6}{m}\right) \tag{2}$$

$$LOQ = 10 \left(\frac{6}{m}\right) \tag{3}$$

2. 2. 9. Selectivity, Stability, and Reproducibility Analysis

In this study, different interfering agents were preferred to confirm the selectivity of designed Boro-S/N -dGQDs for sialic acid in the complex sample containing agents. In brief, diverse types of interfering agents such as NaCl, KCl, uric acid, MgSO₄, and ferric chloride were added into the separate test tube containing pH 7.4 phosphate buffer (100 ng/mL). After this preparation step, 100 μ L of each interfering agent was added to the 5 mL of Boro-S/NdGQDs in a separate test tube. After 10 min, each sample was examined for change in fluorescence using a spectrofluorometer (n = 3). Similarly, 100 ng/mL of sialic acid (100 µL) was added to the 5 mL of Boro-S/N-dGQDs to compare the selectivity in the presence of other interfering substances. In addition, the stability of fluorescence of Boro-S/N-dGQDs was studied at different time points at 25 °C. Similarly, the stability analysis of Boro-S/N-dGQDs as a sensor in the presence of sialic acid was confirmed. In this study, 100 ng/mL of sialic acid was added to the 5 mL of Boro-S/N-dGQDs sensor solution (n = 3). After completion of the redox reaction, the sensor was subjected to confirm the fluorescence quenching at different time intervals at controlled room temperature (25 °C). After this analysis, the reproducibility of the anticipated Boro-S/NdGQDs-based fluorescent sensor was confirmed. In brief, 100 ng/mL of sialic acid was added to the 5 mL of Boro-S/N-dGQDs (n = 6) in triplicate. This sensor was examined for fluorescence quenching in the occurrence of the same concentrations of sialic acid. Here, the percent relative standard deviation (% RSD) was calculated to confirm the stability and reproducibility of the Boro-S/N-dGQDs sensor for the recognition of sialic acid.

2. 2. 10. Real-time Analysis of Sialic Acid

The real-time analysis of sialic acid in local milkbased products, such as cheese, flavored milk, yogurt, and butter was accomplished using a designed fluorescence-based Boro-S/N-dGQDs sensor. In brief, the milk products were collected from the North Maharashtra state. After that, 10 mg of each milk-based product (cheese) was mixed with dilute hydrochloric acid (45 mM) in separate 50 mL of water in a glass beaker for 75 min at 80 °C. Here, hydrolyzation using dilute hydrochloric acid gives the free form of sialic acid from their conjugates.29 Next, 0.1 mL of the sample was added to the test containing 5 mL of Boro-S/N-dGQDs (n = 3), separately. After 5 min, the fluorescence of the sensor was monitored to ensure the quenching of fluorescence due to the presence of sialic acid in the milk product. At last, the sialic acid concentration was calculated using a calibration curve containing the slope and intercept. A similar method was used for other reported milk products such as yogurt, butter, and flavor milk29.

3. Results and Discussion

The bone meal underwent PXRD and EDAX analyses (Figure S1). In Figure S1A, the diffractogram revealed

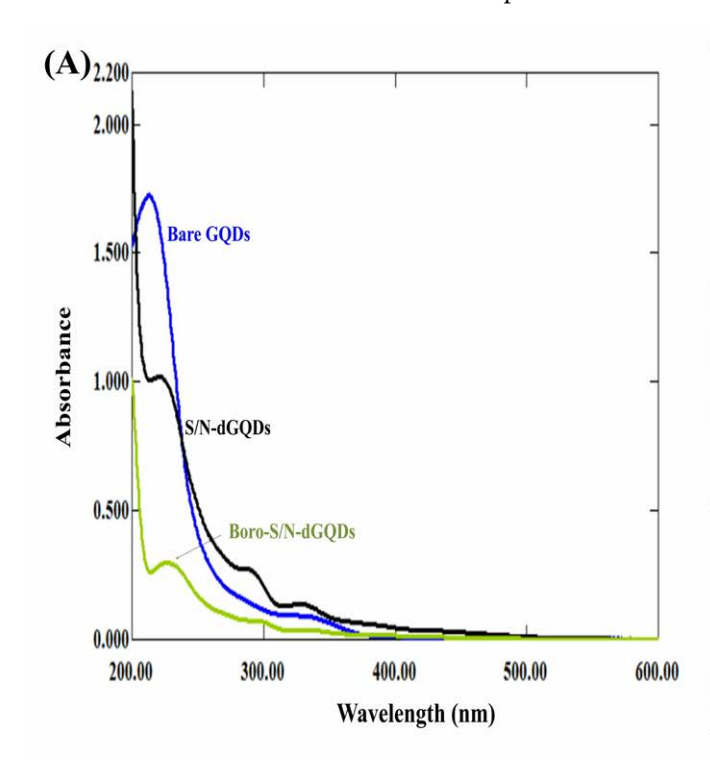




Figure 1: (A) UV Vis spectra of bare GQDs, S/N-dGQDs, and Boro-S/N-dGQDs. (B) UV cabinet pictures of bare GQDs, S/N-dGQDs, and Boro-S/N-dGQDs at visible light (i), short wavelength ($\lambda_{max} = 254 \text{ nm}$ -ii), and long wavelength ($\lambda_{max} = 365 \text{ nm}$ -iii).

sharp intense peaks at 2θ values of 19.94° , 20.64° , 23.56° , 26.38° , 32.32° , 40.19° , 47.28° , etc., indicating its crystalline nature. The EDAX spectrum in Figure S1A displayed the elemental composition of the bone meal, showing the presence of carbon (C), nitrogen (N), oxygen (O), phosphorus (P), sulfur (S), and calcium, constituting 40.77 wt%, 12.84 wt%, 9.49 wt%, 1.08 wt%, 3.45 wt%, respectively. In summary, EDAX analysis confirmed the diverse elemental composition present in the bone meal.

3. 1. UV Vis Spectroscopy

Figure 1A represents the UV Vis spectra of bare GQDs, S/N-dGQDs, and Boro-S/N-dGQDs. In brief, the green-prepared GQDs showed two absorption peaks. Herein, the peak at 215 nm confirmed the π - π * transition of C=C while the peak at 335 nm indicates the n- π^* of -C=O and -OH. Overall, it verifies the presence of carboxylic functional groups in bare GQDs. In the second spectra, the UV Vis spectrum of S/N-dGQDs showed the peaks at 222 nm while it also demonstrates the decreased absorption peaks around 292 nm (π - π * transition of C=C bond) and 330 nm (n- π * transition of C=N, -C=O and -OH). Therefore, it confirmed the presence of amine and carboxylic functionality on the surface of doped GQDs. As well, the no absorption peak for 'S' at near about 550 nm to 595 nm was found, which may be because of the identical electronegativity of 'C' and 'S'. In conclusion, it confirmed the synthesis of S/N-dGQDs using a bone meal via the hydrothermal method.^{30,31} In the case of third spectra, the UV Vis absorption spectra of Boro-S/N-dGQDs displayed two peaks around wavelengths 226 nm and 340 nm, which are ascribed to the π - π * and n- π * transitions of carboxylic and amine functionality, respectively. In these spectra, the reduction in peak intensity at 292 nm was obtained which may be because of structural changes. Furthermore, the shift in UV absorption peaks from 222 nm and 330 nm to 226 nm and 340 nm was obtained, which may be because of functionalization using 4-CPBA. Overall, the UV Vis analysis confirmed the synthesis of Boro-S/N-dGQDs.

3. 2. Fluorescence study of GQDs, S/N-dGQDs, and Boro-S/N-dGQDs

Figure 1B depicts the fluorescence of bare GQDs using a UV cabinet. In brief, the freshly prepared solutions of bare GQDs, S/N-dGQDs, and Boro-S/N-dGQDs were analyzed for changes in fluorescence in different lights. In brief, bare GQDs exhibited no color (transparent), faintly blue, and blue fluorescence at visible light, short wavelength ($\lambda_{\rm max} = 254$ nm), and long wavelength ($\lambda_{\rm max} = 365$ nm), respectively. Figure 1B displays the pictures of the S/N-dGQDs in different lights. In concise, it shows a slight orange color, green luminescence, and prominent blue fluorescence in the visible range, short wavelength ($\lambda_{\rm max} = 254$ nm), and long wavelength ($\lambda_{\rm max} = 365$ nm), respec-

tively. At this instant, it confirmed the significant increment in the fluorescence behavior of S/N-dGQDs. Figure 1B demonstrates the fluorescence behavior of Boro-S/NdGQDs in different lights. In brief, it shows the orange color, greenish-orange fluorescence, and bright bluish fluorescence under visible light, short wavelength ($\lambda_{max} = 254$ nm), and long wavelength ($\lambda_{\text{max}} = 365 \text{ nm}$), respectively. Here, the functionalization of S/N-dGQDs using 4-CPBA offered a boost in the fluorescence property of Boro-S/NdGQDs more than the S/N-dGQDs and bare GQDs. In a nutshell, this study confirmed the functionalization of S/N-dGQDs. After confirmation of fluorescence changes of prepared bare GQDs, S/N-dGQDs, and Boro-S/N -dGQDs, the spectrofluorometer was preferred to ensure the fluorescence characteristic of bare GQDs, S/N-dGQDs, and Boro-S/N-dGQDs. In brief, the diverse types of modification strategies such as doping and functionalization of bare GQDs resulted in the boost in fluorescence properties of GQDs. The % QY was found to be 8.9 %, 25.36 %, and 68.69 % for bare GQDs, S/N-dGQDs, and Boro-S/N -dGQDs, accordingly. Herein, the augment in % QY of Boro-S/N-dGQDs confirmed the improvement in optical properties such as the fluorescence of the sensor. Figure 2A depicts the excitation wavelength-dependent emission spectra of Boro-S/N-dGQDs. In brief, the change in excitation wavelength from 310 nm to 350 nm resulted in a shift in the emission wavelength of Boro-S/N-dGQDs towards a longer wavelength. At an excitation wavelength of 360 nm, it demonstrated an intense emission peak at 425 nm. After an increment in excitation wavelength from 360 nm to 370 nm, the reduction in emission peak with a slight shift towards a longer wavelength was obtained. Overall, the excitation and emission of Boro-S/N-dGQDs were obtained at 360 nm and 425 nm, respectively (Figure 2B). Figure 2C displays the fluorescence behavior of GQDs, S/N-dGQDs, and Boro-S/N-dGQDs. Here, there was a significant difference in the fluorescence behavior of Boro-S/N-dGQDs obtained as compared to the S/N-dGQDs and bare GQDs. Interestingly, it may be because of the combined benefits of 'S' and 'N' atom doping in graphitic structure as well as the functionalization of S/N-dGQDs using 4-CPBA. Overall, Boro-S/N-dGQDs presented a highly fluorescent sensing system for the revealing of interest analytes that can assist in improving sensitivity parameters.

3. 3. pH study of Boro-S/N-dGQDs

The UV cabinet study of Boro-S/N-dGQDs at different pH at longer wavelength light (λ_{max} = 365 nm) reveals the changes in fluorescence behavior. Figure 3A illustrates the UV cabinet pictures of Boro-S/N-dGQDs at different pH ranges. In brief, the change in pH from pH 3 to pH 5 displayed an increase in the fluorescence intensity of Boro-S/N-dGQDs. On the contrary, the adjustment in pH from pH 9 to pH 11 demonstrated the reduction in fluorescence

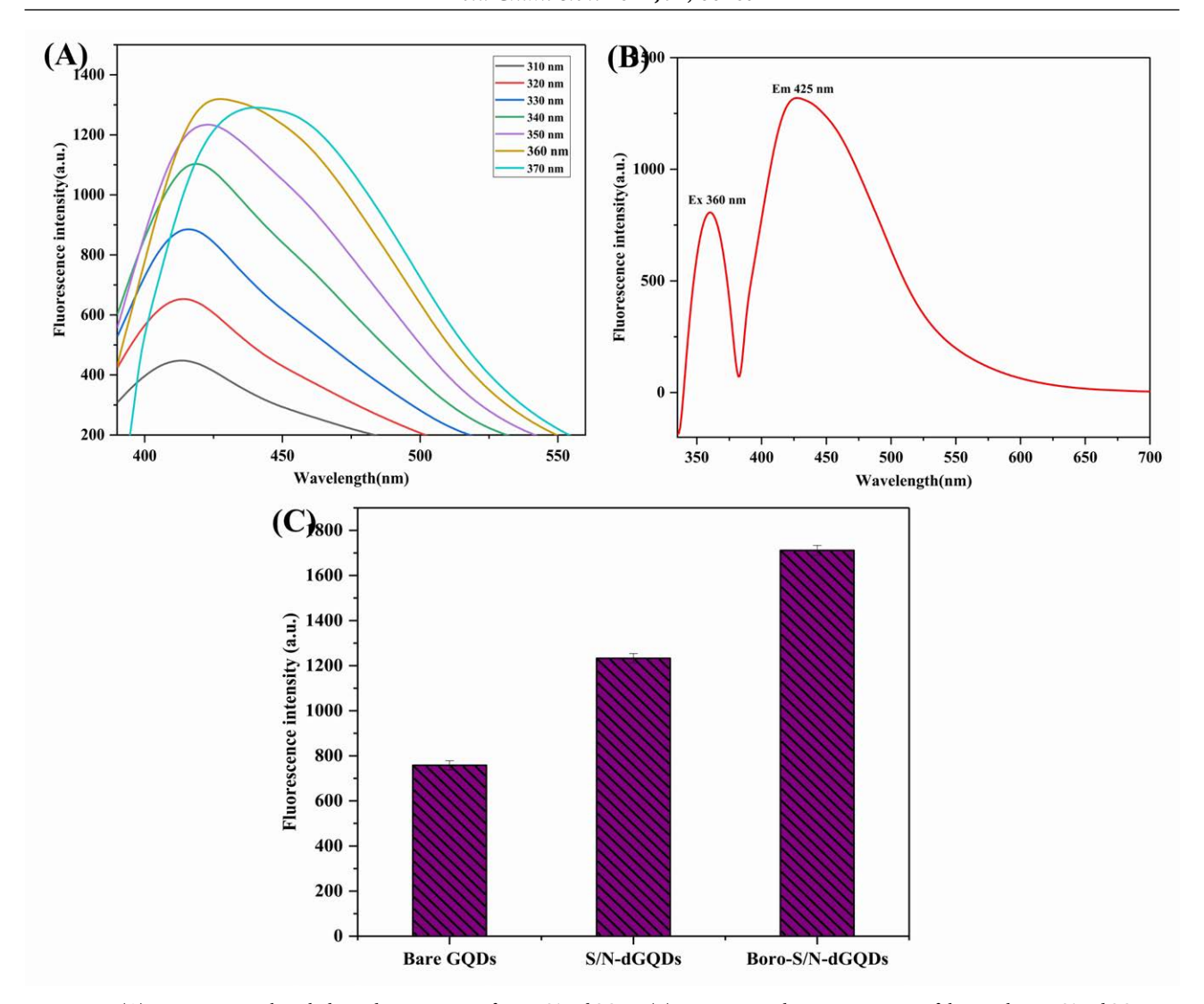


Figure 2: (A) Excitation wavelength dependant emission of Boro-S/N-dGQDs. (B) Excitation and emission spectra of designed Boro-S/N-dGQDs. (C) Fluorescence comparison of bare GQDs, S/N-dGQDs, and Boro-S/N-dGQDs

intensity of Boro-S/N-dGQDs. As well, at pH 7, Boro-S/NdGQDs displayed a high fluorescent intensity. The impact of different pH ranges on the fluorescence property of designed Boro-S/N-dGQDs may be because of protonation and deprotonation. In conclusion, it confirmed the impact of pH on the fluorescence characteristics of Boro-S/N -dGQDs. After qualitative confirmation, the quantitative confirmation of pH impact on fluorescence was confirmed using a spectrofluorometer. Later, the impact of pH of fluorescence of Boro-S/N-dGQDs was examined using a spectrofluorometer (Figure 3B). In concisely, the fluorescence spectra revealed a rise in fluorescence after adjusting the pH from the acidic range (pH 3 to pH 5). At pH 7, the fabricated Boro-S/N-dGQDs sensor disclosed a higher fluorescence intensity. After that, with the change in pH from pH 9 to pH 11 (basic), there was a reduction in fluorescence intensity of the Boro-S/N-dGQDs sensor. Possibly, the protonation or de-protonation and aggregation of the Boro-S/N-dGQDs may be responsible for the pH-based

changes in the fluorescence properties of Boro-S/N -dGQDs.32 Figure 3C disclosed the impact of pH on the zeta potential of the Boro-S/N-dGQDs sensor solution. In concisely, the zeta potential of the Boro-S/N-dGQDs sensor was found to be + 30.58 mV, and + 15.28 mV, for pH 3, and pH 5, accordingly. After changes in pH from the neutral to the basic, the zeta potential of Boro-S/N-dGQDs was obtained to be -34.8 mV, -26.4 mV, and -39.88 mV at pH 7, 9, and 11, respectively. In this, the change in the zeta potential of Boro-S/N-dGQDs with respective adjusted pH of solution confirmed the protonation and deprotonation of carboxylic functionality present in the exterior of Boro-S/N-dGQDs. As well, it ensured the good stability of designed Boro-S/N-dGQDs in an aqueous environment.

3. 4. Zeta Potential and Particle Size Analysis

The zeta potential of nanomaterials is measured to ensure their stability in a particular solvent solution.

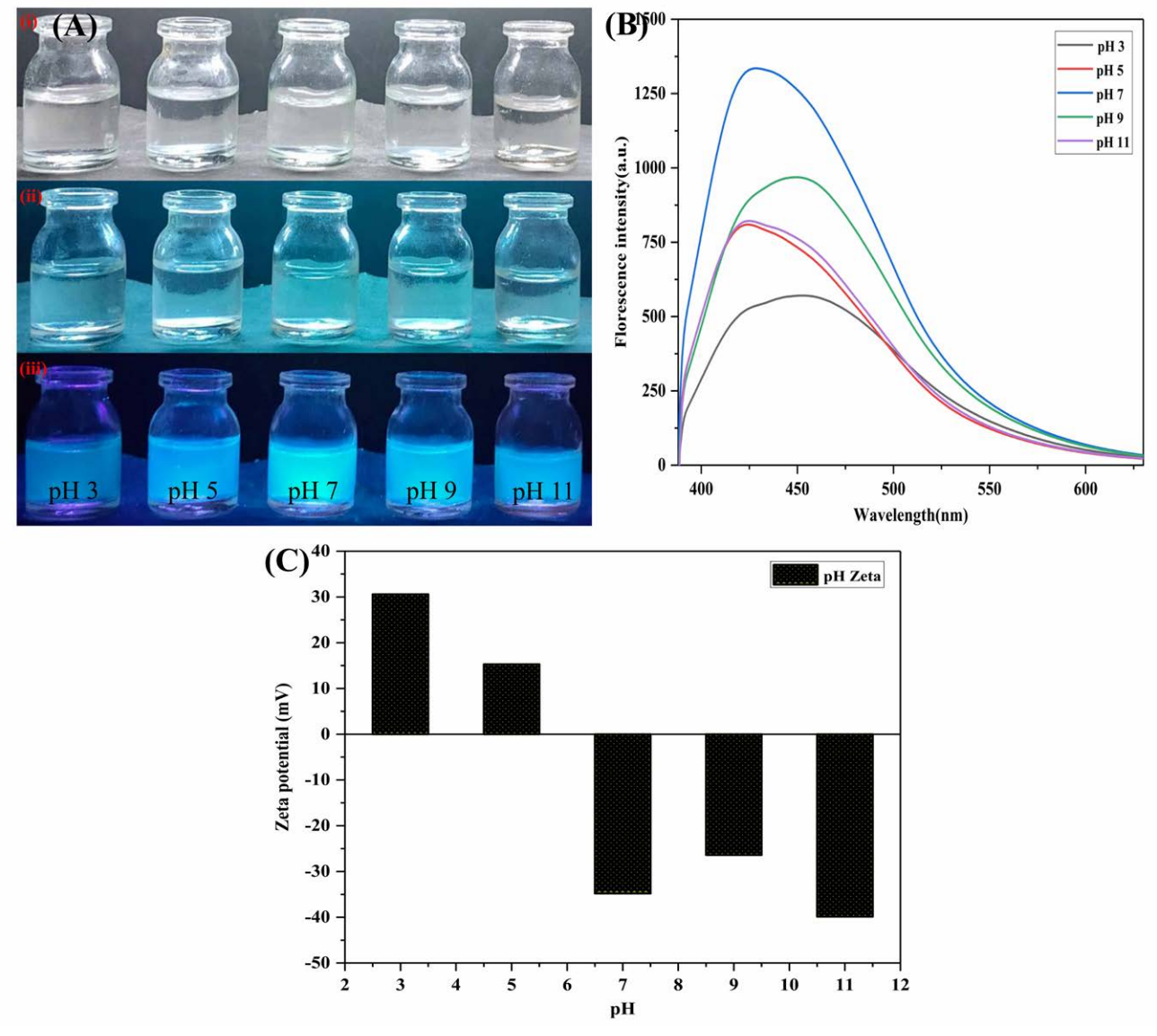


Figure 3: Impact of pH on fluorescence behavior of Boro-S/N-dGQDs. (B) Fluorescence spectra of Boro-S/N-dGQDs in different pH solutions. (C) Zeta potential of Boro-S/N-dGQDs at different pH

Figure 4 depicts the zeta potential of bare GQDs, Boro-S/N-dGQDs, and Boro-S/N-dGQDs.³³ In concisely the zeta potential of citric acid-produced bare GQDs was determined to be -31.79 mV. As a result, it proved that the negative zeta potential was due to the presence of carboxylic functionality on the surface of GQDs, such as carboxyl, hydroxyl, epoxy, etc. It also ensured the stability of GQDs in the aqueous system. The zeta potential of S/N-dGQDs was also discovered to be -20.96 mV. Here, the decrease in zeta potential is caused by the incorporation of 'N' and 'S' into the graphitic structure of GQDs. Furthermore, it demonstrated the stability of S/N-dGQDs in aquatic environments. Boro-S/NdGQDs had a zeta potential of -19.62 mV after the functionalization of the S/N-dGQDs. As a result, it implies that Boro-S/N-dGQDs are stable in specific solvent systems.

3. 5. FT-IR Spectroscopy Analysis

Figure 5A displays the FT-IR spectrum of bare GQDs, S/N-dGQDs, and Boro-S/N-dGQDs. In brief, the peak intensity at 3236 cm⁻¹, 1637 cm⁻¹, 1524 cm⁻¹, 1445 cm⁻¹, 1395 cm⁻¹, and 1233 cm⁻¹ indicates the OH stretching, C=O stretching, aromatic C=C stretching, OH bending, C-O stretching of COOH, and C-O-C stretching vibrations, respectively. Hence, it confirmed the presence of carboxylic functionality in citric acid-made bare GQDs. The peak intensity at 3186 cm⁻¹, 3045 cm⁻¹, 1680 cm⁻¹, 1355 cm⁻¹, and 1170 cm⁻¹ confirmed the OH/NH₂ stretching, -CH stretching, C=O stretching, C-N stretching, and C-S stretching vibrations, respectively. On the whole, the FT-IR analysis confirmed the presence of carbon, oxygen, nitrogen, and sulfur-based functionality in S/N-dGQDs. The peak intensity at 3275 cm⁻¹, 2975 cm⁻¹, 1700 cm⁻¹, 1555 cm⁻¹, 1338 cm⁻¹, 1254 cm⁻¹, and 1170 cm⁻¹ desig-

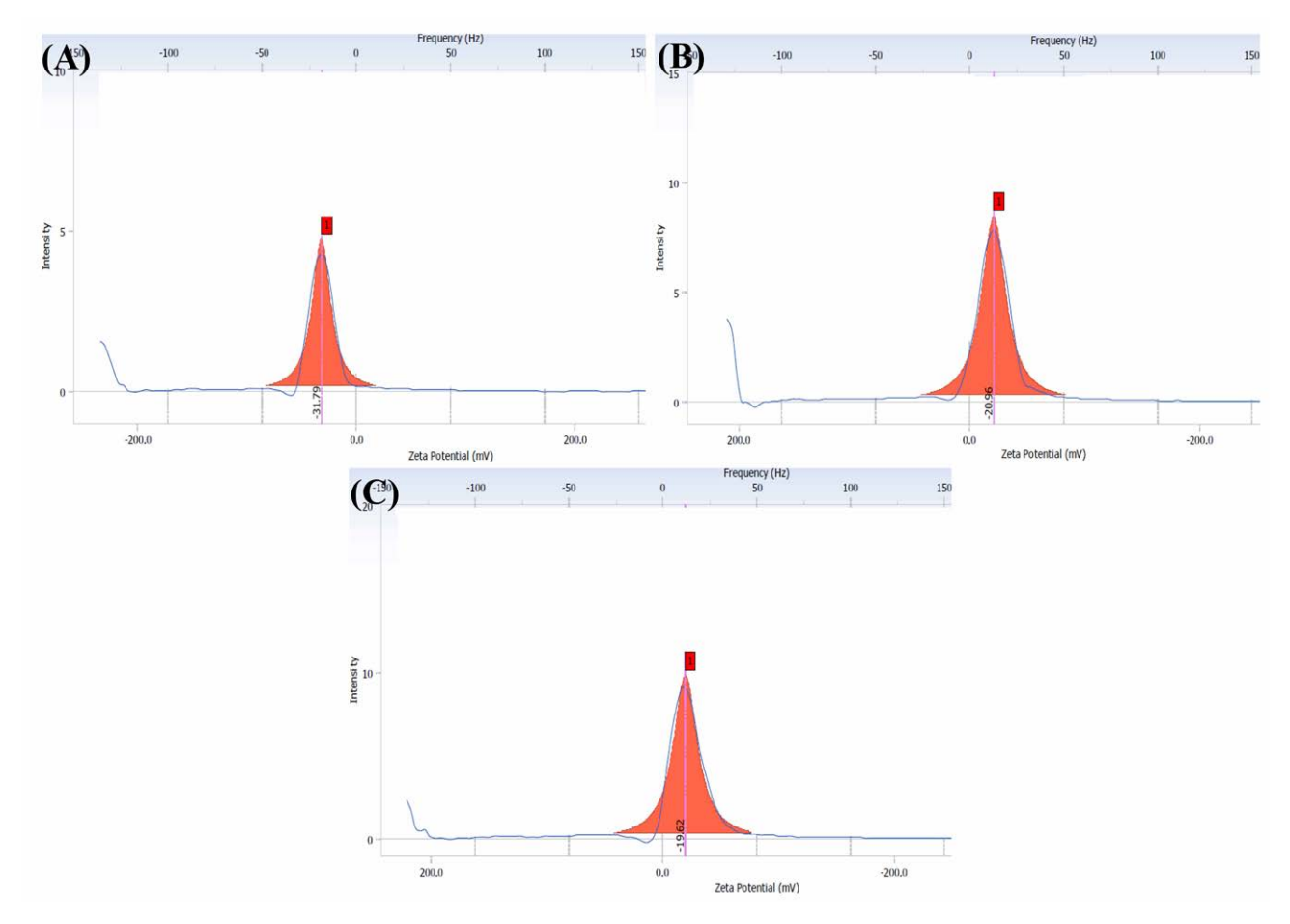
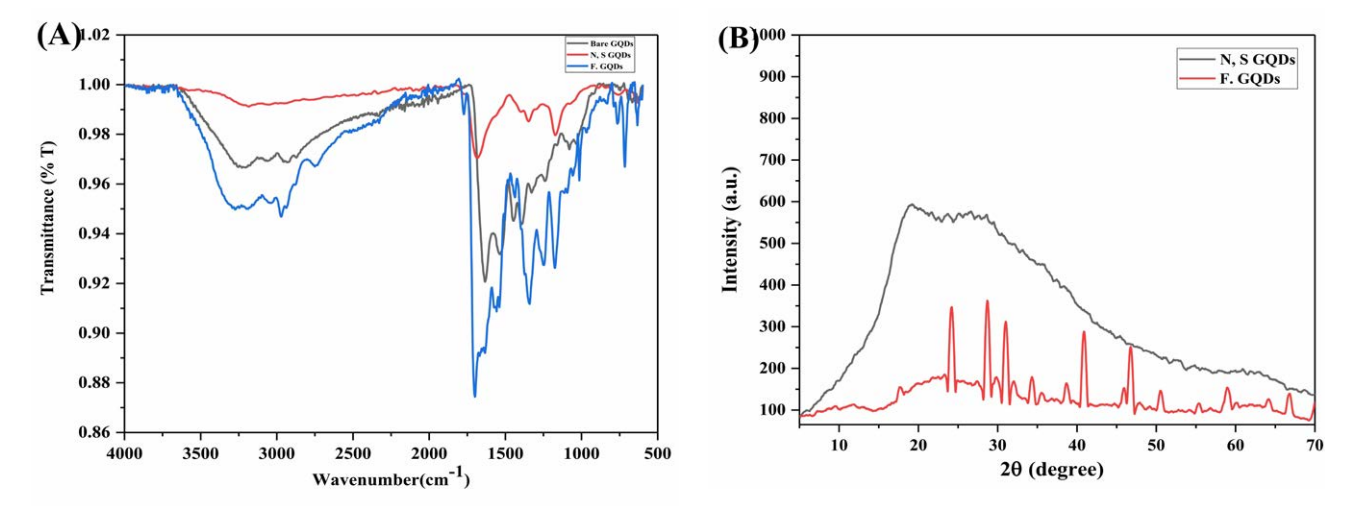


Figure 4: Zeta Potential analysis of (A) bare GQDs, (B) S/N-dGQDs, and (C) Boro-S/N-dGQDs

nates the -OH/NH stretching, C-H stretching, C=O stretching, C-N stretching, B-O-H bending, C-O-C stretching, and C-S stretching vibrations, respectively. Overall, FT-IR analysis confirmed the synthesis of Boro-S/N-dGQDs.

3. 6. Powder X-ray Diffraction (PXRD)

In this work, PXRD analysis ensured the fabrication of the graphitic architecture of S/N-dGQDs and Boro-S/N-dGQDs. In brief, Figure 5B reveals the diffractogram of



 $\textbf{Figure 5:} (A) \ Overlay \ of \ FTIR \ spectra \ of \ overlay \ of \ bare \ GQDs, S/N-dGQDs, \ and \ Boro-S/N-dGQDs. \ (B) \ Diffractogram \ of \ S/N-dGQDs \ and \ Boro-S/N-dGQDs \ and \ Boro-S/N-dGQDs$

S/N-dGQDs in which a wide diffraction peak was obtained at $2\theta = 19.25^{\circ}$ and $23.69^{\circ}.^{30}$ Here, it confirmed the occurrence of S/N-dGQDs in the amorphous form of a

graphene-like structure. Possibly, the doping of the 'N' and 'S' components in graphitic structure enhanced the lattice voids and structural defects. The diffractogram of Boro-S/

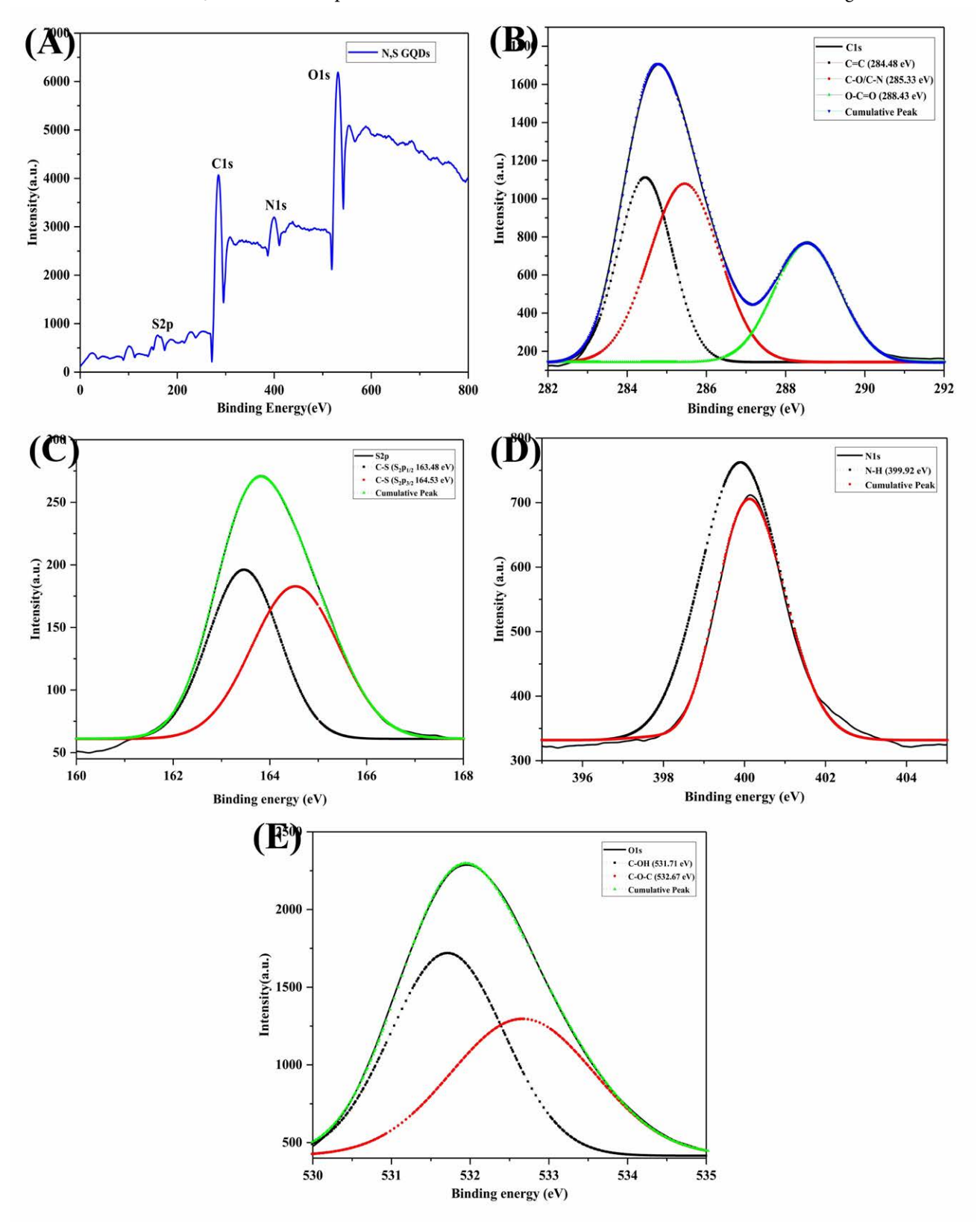


Figure 6: (A) XPS survey scan spectra of S/N-dGQDs. The deconvoluted high-resolution XPS spectra of (B) C1s, (C) S2p, (D) N1s, and (E) O1s

N-dGQDs is presented in Figure 5B. It displays the peaks at $2\theta = 17.70^{\circ}$, 24.19° , 28.70° , 29.99° , 31.02° , 32° , 34.31° , 35.52° , 36.72° , 38.74° , 40.87° , 46.04° , 46.74° , 47.29° , 50.54° , 55.36° , 59.05° , 60.36° and 66.75° . Here, the crystallinity of S/N-dGQDs was increased after functionalization by

4-CPBA ('d' spacing: 0.36). Possibly, the functionality of 4-CPBA provides the separation of graphitic flakes that may part in a boost in the crystalline nature of the sensor. Overall, it confirmed the synthesis of Boro-S/N-dGQDs from S/N-dGQDs.

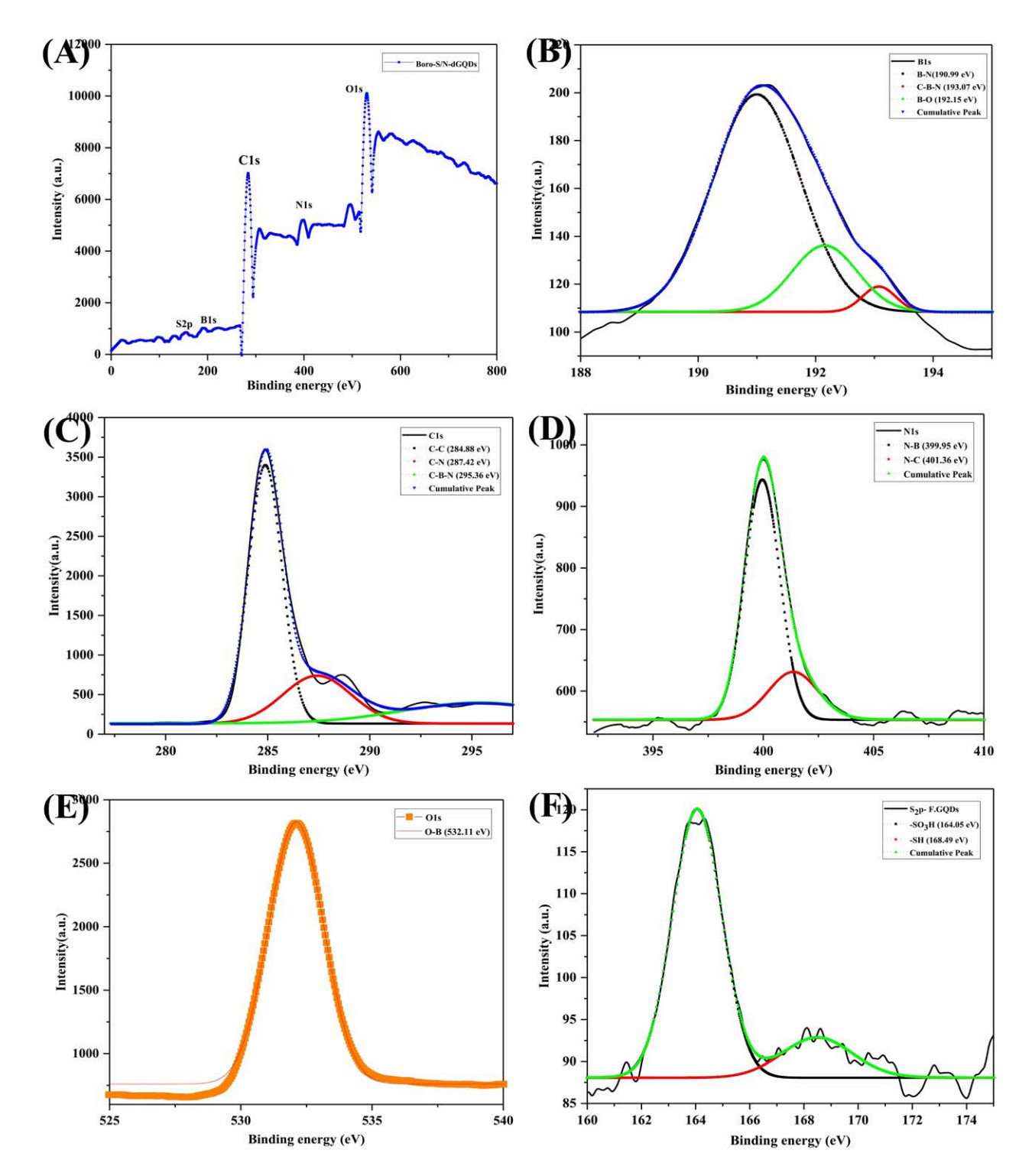


Figure 7: (A) XPS survey scan of Boro-S/N-dGQDs. The deconvoluted high-resolution XPS spectra of (B) B1s, (C) C1s, (D) N1s, (E) O1s, and (F) S2p

3. 7. X-Ray Photoelectron Spectroscopy

Figure 6 represents the XPS spectra of S/N-dGQDs. The survey scan spectrum showed the peaks at binding energy 159.5 eV, 285 eV, 400.5 eV, and 531.5 eV for 'S2p, C1s, N1s, and O1s,' respectively. Hence, it confirmed the presence of 'S, C, N, and 'O'-based functionality in S/N-dGQDs.³⁴ In brief, 'Cls' deconvoluted high-resolution peaks showed the binding energies at 284.48 eV, 285.33 eV, and 288.43 eV for C=C, C-O/C-N, and O-C=O respectively. As a result, it assured the presence of carbon-based functionality in S/N-dGQDs. The 'O1s' deconvoluted high-resolution XPS spectra demonstrated the intensity

peaks at binding energies of 531.71 eV and 532.67 eV for C-OH and C-O-C, respectively. Hence, it confirmed the existence of oxygen-based functionality in S/N-dGQDs. The 'S2p' deconvoluted high-resolution XPS spectra showed peaks at binding energies of 163.48 eV and 163.53 eV for C-S (S2p_{1/2}) and C-S (S2p_{3/2}), respectively. Hence, it verified the doping of the 'S' element into the graphitic structure of GQDs. The 'N1s' high-resolution peaks illustrated the binding energies at 399.92 eV for N-H that ensured the presence of 'N' in graphitic frameworks of GQDs. In conclusion, the XPS analysis of S/N-dGQDs validated the synthesis of heteroatom-doped GQDs from

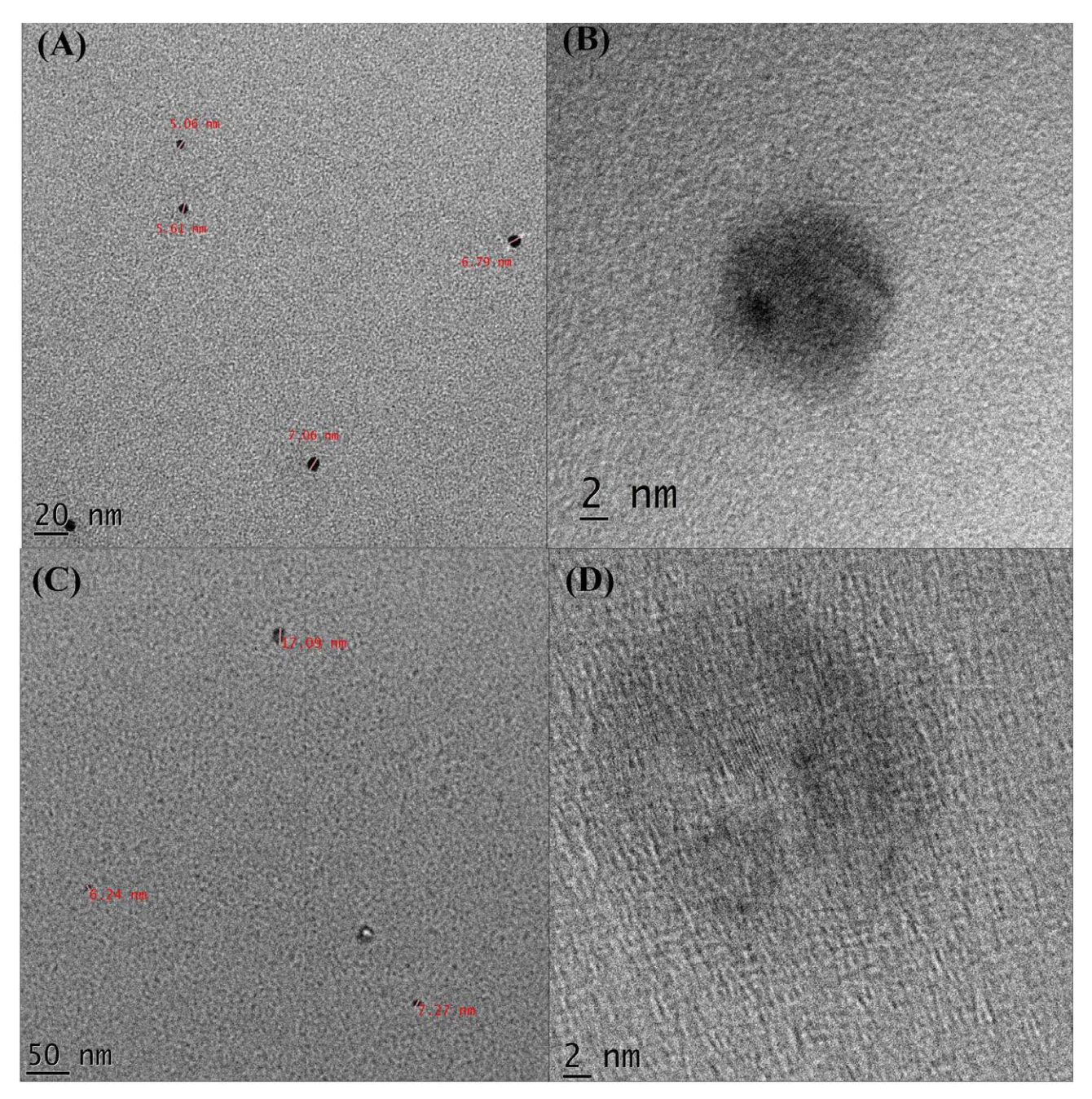


Figure 8: HR-TEM images of (A, B) S/N-dGQDs and (C, D) Boro-S/N-dGQDs

bone meal. Figure 7 represents the XPS spectra of Boro-S/ N-dGQDs. The survey scan spectrum of Boro-S/N-dGQDs displayed the major peaks at near about 154 eV, 192.5 eV, 284 eV, 399 eV, and 531.5 eV indicating the S2p, B1s, C1s, N1s, and O1s, respectively. Hence, it confirmed the occurrence of 'B1s, S2p, C1s, N1s, and O1s' after the functionalization of S/N-dGQDs.34 In brief, the 'S2p' deconvoluted high-resolution XPS spectra demonstrated the peaks at the binding energies of 164.05 eV and 168.49 eV for -SO₃H and -SH, respectively. The 'B1s' deconvoluted high-resolution XPS spectra disclosed the peaks at binding energies of 190.99 eV, 193.07 eV, and 192.15 eV for B-N, C-B-N, and B-O, respectively. Therefore, it confirmed the functionalization of S/N-dGQDs using 4-CPBA. In short, the 'Cls' deconvoluted high-resolution XPS spectra revealed the binding energies at 284.88 eV, 287.42 eV, and 295.36 eV for C-C, C-N, and C-B-N, respectively. The 'O1s' deconvoluted high-resolution XPS spectra showed the peaks at 532.11 eV for O-B and C-O confirming the presence of oxygen-based functionality. In addition, the 'N1s' deconvoluted high-resolution XPS spectra endow with the peaks at binding energies of 399.95 eV and 401.36 eV for N-B and N-C, respectively. Consequently, it confirmed the functionalization of S/N-dGQDs using 4-CPBA.

3. 8. HR-TEM Analysis

The particle size and shape of S/N-dGQDs and Boro-S/N-dGQDs were confirmed using HR-TEM analysis. In brief, Figures 8A and B displayed the HR-TEM images of S/N-dGQDs. In this, the average particle size of S/NdGQDs was found to be less than 10 nm. As well, the shape of S/N-dGQDs was found to be spherical with proper distribution in the aqueous system. Overall, it confirmed the synthesis of nanosized and non-aggregated S/N-dGQD.³⁵ Figures 8C and D illustrate the HR-TEM image of Boro-S/N-dGQDs. Here, the average particle size of Boro-S/NdGQDs was found to be upto 20 nm. As well, it depicts the spherical shape along with homogenous dispersion in an aqueous environment. Here, the increase in average particle size of Boro-S/N-dGQDs was obtained from the S/NdGQDs which may be because of the decoration of 4-CPBA on the surface of S/N-dGQDs. Taken as a whole, the HR-TEM analysis proved the synthesis of nano dimension and uniform distribution of Boro-S/N-dGQDs from bone meal.³⁵

3. 9. Raman Spectroscopy

Figure 9 depicts the Raman spectra of as-synthesized S/N-dGQDs and Boro-S/N-dGQDs. In brief, the Raman spectra of S/N-dGQDs revealed the two bands namely the 'D' band and the 'G' band at near about 1327.77 cm⁻¹ and 1583.39 cm⁻¹ respectively. The ratio of the intensity of the 'D' band and the 'G' band (I_D/I_G) was obtained to be 1.64. Here, the disordered structure of the

'D' band is related to hetero-atom doping faults and size reduction. On the contrary, the crystal-like character of carbon material is accompanied by the 'G' band. 36,37 In the case of Raman spectra of Boro-S/N-dGQDs, the 'D' band, and the 'G' band were obtained at 1327.70 cm⁻¹ and 1587.44 cm⁻¹, respectively. The ratio of I_D/I_G (I_D/I_G :1.14) was found to be reduced than the S/N-dGQDs, which may be because of the functionalization of S/N-dGQDs, surface using 4-CPBA. 36,37 Overall, the Raman analysis confirmed the synthesis of S/N-dGQDs and Boro-S/N-dGQDs.

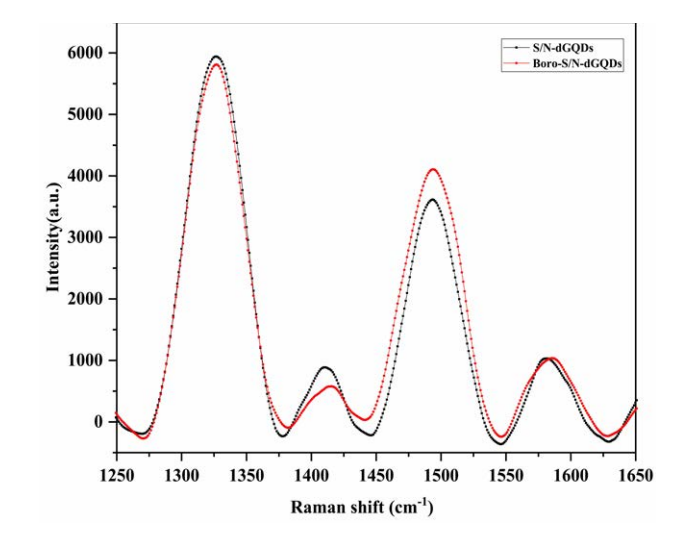


Figure 9: Raman spectra of S/N-dGQDs and Boro-S/N-dGQDs.

3. 10. Sensing of Sialic Acid using Fluorescence-Based Boro-S/N-dGQDs

In this step, sialic acid was detected using a fabricated highly fluorescent Boro-S/N-dGQDs sensor. To begin, different concentrations of sialic acid were incubated in a separate test tube containing the Boro-S/N-dGQDs sensor. Here, the reaction between sialic acid and 4-APBA of functionalized doped GQDs was achieved. As an output, the screening of fluorescence of the Boro-S/N-dGQDs sensor in the occurrence of sialic acid revealed fluorescence quenching. Similarly, an increase in sialic acid concentration has a directly proportional relationship with fluorescence suppression of the Boro-S/N-dGQDs sensor (Figure 10A). The linearity range $(y = 6.71x + 0.1089, R^2 =$ 0.99) of sialic acid appears here from 50 ng/mL to 1000 ng/ mL (Figure 10B). The LOD and LOQ for sialic acid were then determined to be 6.04 ng/mL and 14.81 ng/mL, respectively. It ensured that the doping of heteroatoms like 'N' and 'S', as well as the boronic acid functionalization of GQDs, provides increased sensitivity to sialic acid. In terms of sensing, the Boro-S/N-dGQDs sensor provides boronic acid functional groups on the surface. Importantly, it generates a reversible covalent contact with sialic acid.

Table 1: Summary of SA detection using fluorescence-mediated sensing methods

Sr. No.	Material used	Method used	LOD	Linearity range	Ref.
1.	Boronic acid functionalized carbon dots	Spectrofluorimetric	54 μΜ	80 μM to 4000 μM	40
2.	Gold nanoparticles	Colorimetric	68 μΜ	80 μM to 2000 μM	41
3.	-	Liquid chromatography fluorescence detection	0.003 mg/ mL	$0.1 \mu g/mL$ to $10 \mu g/mL$	42
4.	_	Spectrophotometric	0.239 mg/mL	1 mg/mL to 10 mg/mL	43
5.	Zirconium metal-organic framework	Spectrofluorimetric	0.15 μΜ	1 μM to 100 μM	44
6.	Boro-S/N-dGQDs	Spectrofluorimetric	6.04 ng/mL	50 ng/mL to 1000 ng/mL	Present work

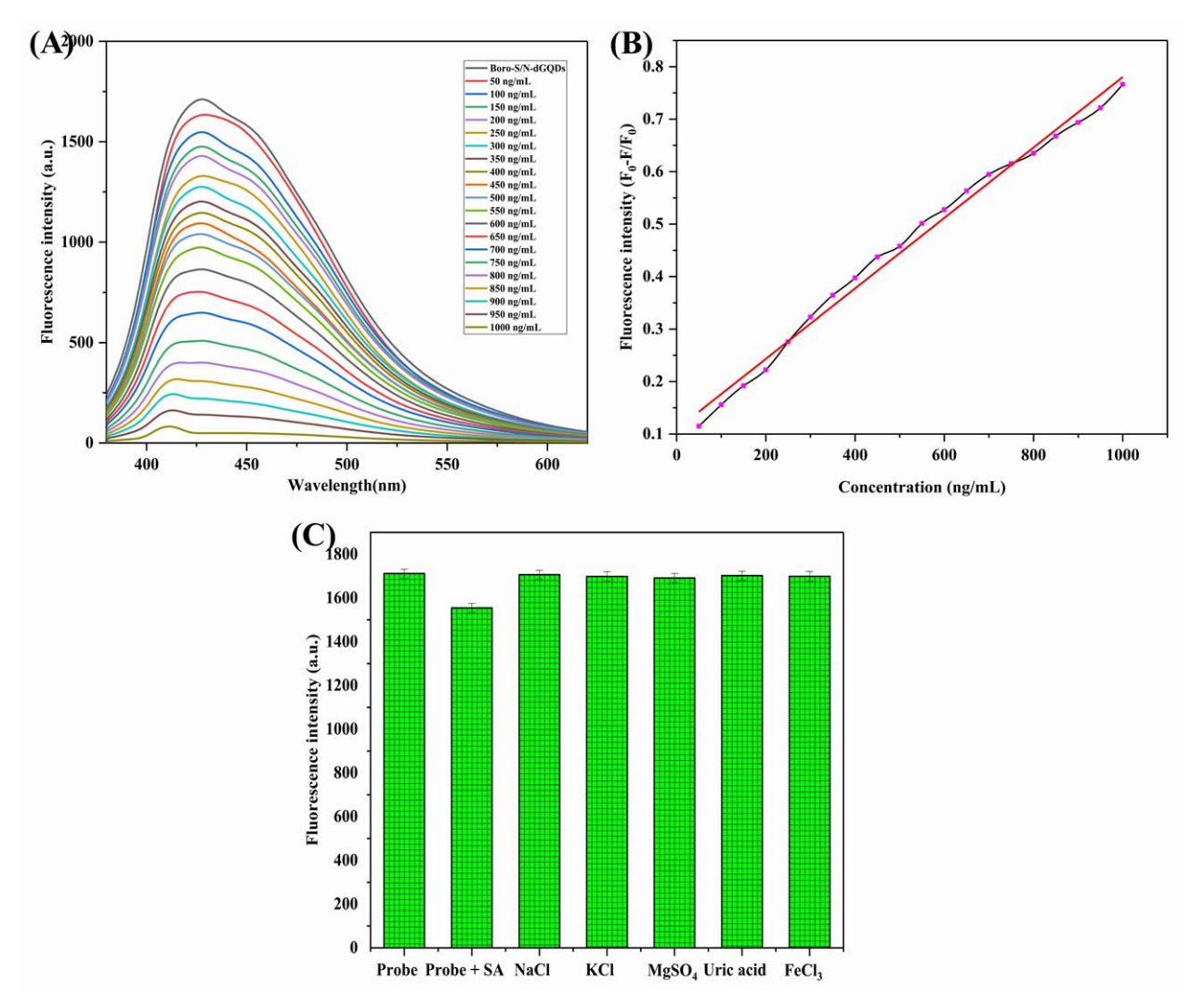


Figure 10: (A) Fluorescence spectra of sialic acid concentrations based on quenching of Boro-S/N-dGQDs fluorescence. (B) Graph of linear correlation between concentrations of sialic acid and fluorescence of Boro-S/N-dGQDs. (C) Selectivity study of Boro-S/N-dGQDs (probe) for sialic acid (SA) in the presence of interfering agents

As a result, it aids in modulating the fluorescence intensity of the Boro-S/N-dGQDs sensor.^{38,39} Table 1 summarizes the comparison of formerly reported methods for sensing sialic acid.

3. 11. Selectivity Study and Other Analytical Parameters

To verify the anti-interference potential of the Boro-S/N-dGQDs sensor, the selectivity study was per-

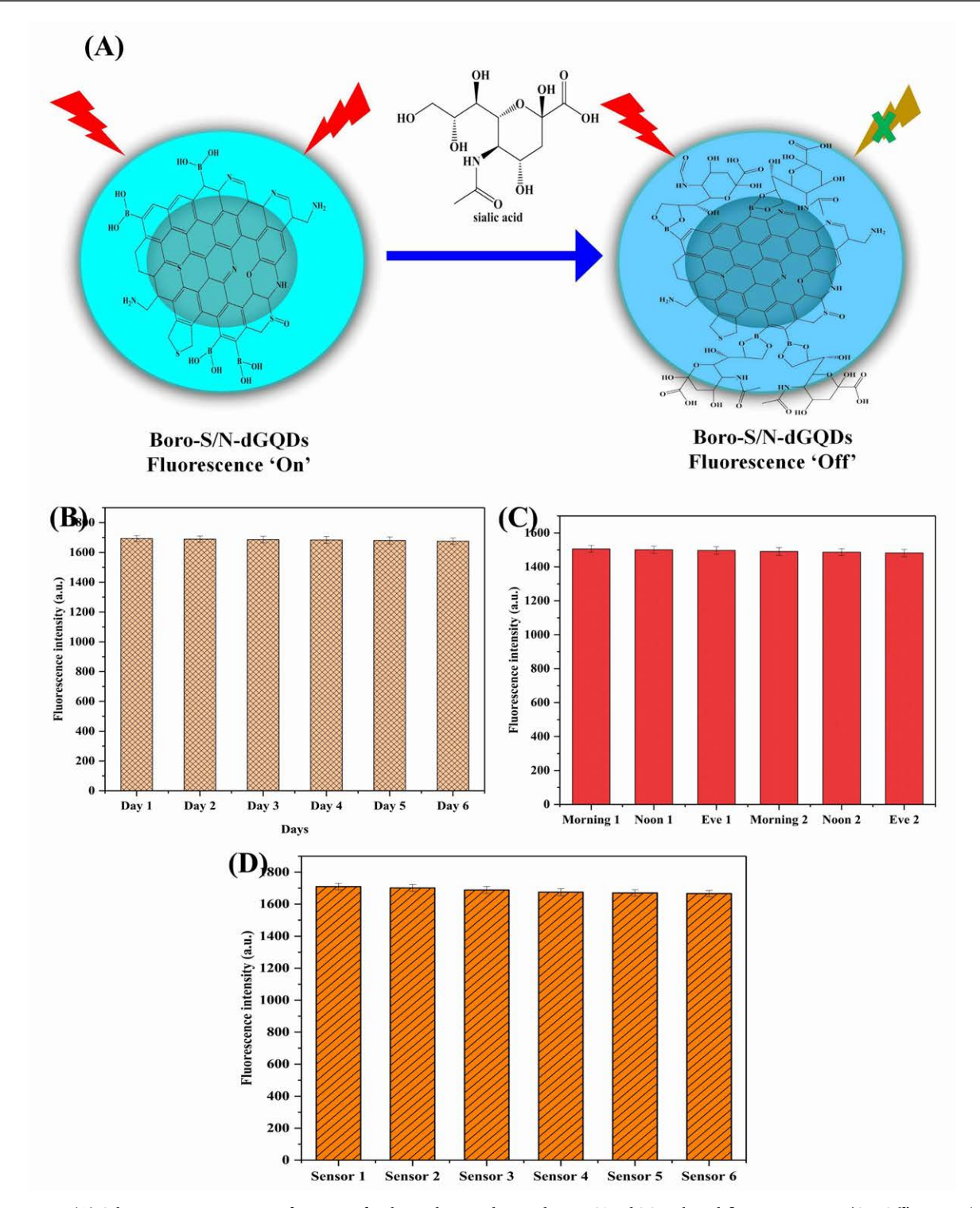


Figure 11: (A) Schematic representation of sensing of sialic acid using designed Boro-S/N-dGQDs based fluorescence turn 'On-Off' sensor. (B) Fluorescence stability of Boro-S/N-dGQDs. (C) Sensor stability of Boro-S/N-dGQDs after the addition of sialic acid at different intervals. (D) Reproducibility study of Boro-S/N-dGQDs for detection of sialic acid (n = 6).

formed using different interfering agents. Figure 10C illustrates the selectivity potential of the Boro-S/N-dGQDs sensor for sialic acid in the occurrence of interfering substances. In short, it verifies the fluorescence quenching of the Boro-S/N-dGQDs sensor after the addition of sialic

acid. On the contrary, there was no response was found for the addition of the mentioned interfering molecules. Moreover, the addition of sialic acid with a mixture of interfering agents did not demonstrate a significant change in fluorescent intensity than the Boro-S/N-dGQDs

sensor with a sialic acid response. Importantly, the fabricated Boro-S/N-dGQDs sensor demonstrated the high selectivity for sialic acid only due to the esterification reaction between boronic acid-containing functional groups and sialic acid. After this, stability and reproducibility analysis was performed as an important analytical parameter of the sensor. The scheme of the detection mechanism for sialic acid using a highly fluorescent Boro-S/N-dGQDs sensor is revealed in Figure 11A. In brief, the boronic functional group of prepared Boro-S/ N-dGQDs formed the cyclic ester with a sialic acid-containing dial group that may be the possible reason for the quenching of fluorescence behavior of Boro-S/N-dGQDs. At first, the fluorescence stability (Figure 11B) was performed in the absence of sialic acid wherein it proved good stability for up to 6 days (n = 3). After this, a decline in fluorescence intensity was obtained, which may be because of the protonation or deprotonation of Boro-S/NdGQDs in the solution. As well, the Boro-S/N-dGQDs sensor stability was performed with sialic acid (Figure 11C). Herein, the addition of sialic acid into the fluorescent Boro-S/N-dGQDs sensor shows the quenching of fluorescence. The stability study ensured that the slight recovery of suppressed fluorescence of Boro-S/N -dGQDs-SA was found after 48 h. Hence, it confirmed the good stability (% RSD: 0.0068%) of Boro-S/N -dGQDs-SA samples. The reproducibility analysis of the Boro-S/N-dGQDs sensor provided the 0.0067% of % RSD (less than 5) confirmed good reproducibility (Figure 11D). Overall, the designed Boro-S/N-dGQDs-based fluorescent sensor exhibited high sensitivity, high selectivity, good stability, and reproducibility for the recognition of sialic acid. In the future, there is a need to conduct spiked sample analysis and preclinical studies to ensure the practical applicability of the proposed Boro-S/N -dGQDs fluorescent-mediated sensor for sensing sialic acid.

3. 12. Real-time Analysis of Sialic Acid

The real-time analysis of sialic acid in local milk-based products was accomplished using a fluorescence Boro-S/N-dGQDs sensor. In summary, the total amount of sialic acid in cheese and butter was found to be 11 ± 1.10 ng/mL and 7.5 ± 1.85 ng/mL, respectively. Similarly, the analysis of flavored milk and yogurt confirmed the presence of 6.4 ± 2.41 ng/mL and 9.74 ± 2.14 ng/mL of sialic acid, respectively. In conclusion, the Boro-S/N-dGQDs sensor confirmed the presence of sialic acid in milk products of north Maharashtra, India. In the future, there is a need to explore the reported Boro-S/N-dGQDs on a larger scale for the detection of sialic acid in different milk products. Furthermore, the validation of the proposed sensor using another method is needed for the detection of sialic acid.

4. Conclusion

This work aimed to construct an extremely luminous Boro-S/N-dGQDs sensor for highly sensitive and selective detection of sialic acid in milk-based products. In concise, the bone meal was effectively used as both a dopant and precursor in the single-step hydrothermal synthesis of S/N-dGQDs, resulting in improved fluorescence compared to bare GQDs. Subsequently, 4-CPBA was used to functionalize the surface of S/N-dGQDs, leading to even higher fluorescence levels than S/N-dGQDs alone. Next, the spectral study confirmed the formation of stable, nanosized, spherical Boro-S/N-dGQDs with appropriate functional groups required for sialic acid detection. Upon the addition of sialic acid to Boro-S/N-dGQDs, the fluorescence exhibited a 'turn ON-OFF' behavior, providing a wide linear range from 50 ng/mL to 1000 ng/mL and a reduced detection limit of 6.04 ng/mL in phosphate buffer at pH 7.4. The sensor also demonstrated strong selectivity for sialic acid due to the interaction of sialic acid-containing 1,2-diol with a hydroxyl group of Boro-S/N-dGQDs. Furthermore, the Boro-S/N-dGQDs design exhibited high stability and repeatability. The real-time analysis confirmed the presence of sialic acid in cheese, butter, flavored milk, and yogurt, thus affirming the practicality of the designed Boro-S/N-dGQDs sensor for detecting and monitoring sialic acid in milk-based products. In conclusion, Boro-S/N-dGQDs offer a highly selective, sensitive, simplistic, eco-friendly, and cost-effective platform for sensing sialic acid in milk-based products. However, before their application in milk product analysis, further confirmation using Boro-S/N-dGQDs will be necessary in the future.

Conflict of interest

The authors disclosed no conflict of interest.

Acknowledgments

Sopan Nangare would like to express their gratitude to the Indian Council of Medical Research (ICMR), New Delhi for providing a Research Associate (RA) fellowship.

5. References

- H. Zhang, H. Yu, M. Deng, Z. Ren, Z. Li, L. Zhang, J. Li, E. Wang, X. Wang, J. Li, *Microchem. J.* 2023, 190, 108676.
 DOI:10.1016/j.microc.2023.108676
- T. Zhang, J. Wu, X. Zhan, Crit. Rev. Food Sci. Nutr. 2023, 1–24. DOI:10.1080/10408398.2023.2202254
- C. H. Röhrig, S. S. Choi, N. Baldwin, Crit. Rev. Food Sci. Nutr. 2017, 57, 1017–1038. DOI:10.1080/10408398.2015.1040113
- V. Padler-Karavani, H. Yu, H. Cao, H. Chokhawala, F. Karp, N. Varki, X. Chen, A. Varki, *Glycobiology* 2008, 18, 818–830. DOI:10.1093/glycob/cwn072

- J. C. Löfling, A. W. Paton, N. M. Varki, J. C. Paton, A. Varki, Kidney Int. 2009, 76, 140–144. DOI:10.1038/ki.2009.131
- T. Liu, B. Fu, J. Chen, Z. Yan, K. Li, Electrochim. Acta 2018, 269, 136–143. DOI:10.1016/j.electacta.2018.02.132
- 7. L. Chen, N. Wang, J. Wu, F. Yan, H. Ju, *Anal. Chim. Acta* **2020**, *1128*, 231–237. **DOI:**10.1016/j.aca.2020.07.006
- 8. G. Broncová, P. Matějka, Z. Němečková, V. Vrkoslav, T. V. Shishkanova, *Electroanalysis* **2018**, *30*, 672–680. **DOI:**10.1002/elan.201700634
- J. Cheeseman, G. Kuhnle, G. Stafford, R. A. Gardner, D. I. Spencer, H. M. Osborn, *Biomark. Med.* 2021, 15, 911–928. DOI:10.2217/bmm-2020-0776
- H. Xie, Y. Lu, R. You, W. Qian, S. Lin, RSC Adv. 2022, 12, 8160–8171. DOI:10.1039/D2RA00337F
- A. S. Gadtya, D. Tripathy, S. Moharana: Biomass-Based Functional Carbon Nanostructures for Supercapacitors, In: Tiwari, S.K., Bystrzejewski, M., Kumar, V. (eds) Biomass-Based Functional Carbon Nanostructures for Supercapacitors. Green Energy and Technology. Springer, 2023, pp. 223–243. DOI:10.1007/978-981-99-0996-4
- M. T. Dejpasand, S. Sharifi, E. Saievar-Iranizad, A. Yazdani, K. Rahimi, *J. Energy Storage* **2021**, *42*, 103103.
 DOI:10.1016/j.est.2021.103103
- T. Van Tam, N. B. Trung, H. R. Kim, J. S. Chung, W. M. Choi, Sens. Actuators B Chem. 2014, 202, 568–573.
 DOI:10.1016/j.snb.2014.05.045
- N. Sohal, B. Maity, S. Basu, RSC Adv. 2021, 11, 25586–25615.
 DOI:10.1039/D1RA04248C
- T. Han, Y. Huang, T. Gao, C. Xia, C. Sun, W. Xu, D. Wang, Food Chem. 2023, 404, 134509.
 DOI:10.1016/j.foodchem.2022.134509
- S. Nangare, S. Baviskar, A. Patil, P. Patil, Acta Chim. Slov. 2022, 69, 437–447. DOI:10.17344/acsi.2022.7333
- 17. M. Ghiyasiyan-Arani, M. Salavati-Niasari, *Sci. Rep.* **2022**, *12*, 8103. **DOI**:10.1038/s41598-022-12321-2
- R. S. Tade, S. N. Nangare, A. G. Patil, A. Pandey, P. K. Deshmukh, D. R. Patil, T. N. Agrawal, S. Mutalik, A. M. Patil, M. P. More, *Nanotechnology* 2020, *31*, 292001.
 DOI:10.1088/1361-6528/ab803e
- H. Kuzhandaivel, S. Manickam, S. K. Balasingam, M. C. Franklin, H.-J. Kim, K. S. Nallathambi, *New J. Chem.* 2021, 45, 4101–4110. DOI:10.1039/D1NJ00038A
- S. Bian, C. Shen, Y. Qian, J. Liu, F. Xi, X. Dong, Sens. Actuators B: Chem. 2017, 242, 231–237.
 DOI:10.1016/j.snb.2016.11.044
- M. Esteves, D. Mombrú, M. Romero, L. Fernández-Werner,
 R. Faccio, A. W. Mombrú, *Mater. Today Electronics* 2023, 3, 100029. DOI:10.1016/j.mtelec.2023.100029
- A. M. Mahmoud, M. H. Mahnashi, S. A. Alkahtani, M. M. El-Wekil, *Int. J. Biol. Macromol.* 2020, *165*, 2030–2037.
 DOI:10.1016/j.ijbiomac.2020.10.084
- Z.-b. Qu, X. Zhou, L. Gu, R. Lan, D. Sun, D. Yu, G. Shi, Chem. Commun. 2013, 49, 9830–9832. DOI:10.1039/c3cc44393k
- C. Zhou, B. Liu, Y. Fang, R. Zhou, L. Qian, S. Tang, S. Ou, R. Cheng, Sens. Actuators B: Chem. 2023, 381, 133441.
 DOI:10.1016/j.snb.2023.133441

- Z. G. Khan, P. O. Patil, *Mater. Chem. Phys.* 2022, 276, 125383.
 DOI:10.1016/j.matchemphys.2021.125383
- S. Nangare, S. Patil, A. Patil, P. Deshmukh, P. Patil, *J. Photochem. Photobiol. A: Chem.* 2023, 438, 114532.
 DOI:10.1016/j.jphotochem.2022.114532
- H. Yu, Y. Li, A. Huang, *Talanta* 2021, 232, 122434.
 DOI:10.1016/j.talanta.2021.122434
- S. Nangare, S. Patil, S. Patil, Z. Khan, A. Patil, P. Patil, *Inorg. Chem. Commun.* 2022, 143, 109751.
 DOI:10.1016/j.inoche.2022.109751
- 29. D. Karunanithi, A. Radhakrishna, V. Biju, *Int. J. Appl. Biol. Pharm. Technol.* **2013, 4,** 318–323. **DOI:** https://www.fortunejournals.com/ijabpt/pdf/57048-V.M.Biju%20(1).pdf
- 30. C. Chen, D. Zhao, T. Hu, J. Sun, X. Yang, Sens. Actuators B: Chem. 2017, 241, 779–788. DOI:10.1016/j.snb.2016.11.010
- 31. Y. Wang, S.-H. Kim, L. Feng, *Anal. Chim. Acta* **2015**, 890, 134–142. **DOI:**10.1016/j.aca.2015.07.051
- 32. S. Lai, Y. Jin, L. Shi, R. Zhou, Y. Zhou, D. An, *Nanoscale* **2020**, *12*, 591–601. **DOI:**10.1016/j.talanta.2021.122434
- 33. T. K. Mondal, D. Dinda, S. K. Saha, Sens. Actuators B: Chem. **2018**, 257, 586–593. **DOI**:10.1016/j.snb.2017.11.012
- L. Sheng, B. Huangfu, Q. Xu, W. Tian, Z. Li, A. Meng, S. Tan, J. Alloys Compd. 2020, 820, 153191.
 DOI:10.1016/j.jallcom.2019.153191
- Q. Wang, L. Li, T. Wu, X. Kong, Q. Ma, C. Ma, Spectrochim. Acta A: Mol. Biomol. Spectrosc. 2020, 229, 117924.
 DOI:10.1016/j.saa.2019.117924
- 36. Y. Yao, C. Xu, J. Qin, F. Wei, M. Rao, S. Wang, *Ind. Eng. Chem. Res.* **2013**, *52*, 17341–17350. **DOI:**10.1021/ie401690h
- S. Gu, C.-T. Hsieh, Y.-Y. Tsai, Y. Ashraf Gandomi, S. Yeom, K.
 D. Kihm, C.-C. Fu, R.-S. Juang, ACS Appl. Nano Mater. 2019, 2, 790–798. DOI:10.1021/acsanm.8b02010
- 38. M. Masteri-Farahani, F. Ghorbani, N. Mosleh, *Spectrochim. Acta A: Mol. Biomol. Spectrosc.* **2021**, 245, 118892. **DOI:**10.1016/j.saa.2020.118892
- H. Fujisaki, A. Matsumoto, Y. Miyahara, T. Goda, Sci. Technol. Adv. Mater. 2022, 23, 525–534.
 DOI:10.1080/14686996.2022.2122867
- S. Xu, S. Che, P. Ma, F. Zhang, L. Xu, X. Liu, X. Wang, D. Song, Y. Sun, *Talanta* 2019, 197, 548–552.
 DOI:10.1016/j.talanta.2019.01.074
- 41. S. Sankoh, C. Thammakhet, A. Numnuam, W. Limbut, P. Kanatharana, P. Thavarungkul, *Biosens. Bioelectron.* **2016**, *85*, 743–750. **DOI:**10.1016/j.bios.2016.05.083
- 42. F. Zhao, B. Chen, K. Li, X. Wang, *Sh Kexue/Food Sci.* **2021**, *42*, 313–318. **DOI:** 10.7506/spkx1002-6630-20191008-031
- J. B. Costa, N. T. de Paula, P. A. da Silva, G. C. de Souza, A. P. S. Paim, A. F. Lavorante, *Microchem J.* 2019, *147*, 782–788.
 DOI:10.1016/j.microc.2019.03.086
- 44. Q. Cao, Y. Peng, Q. Yu, Z. Shi, Q. Jia, *Dyes Pigm.* **2022**, *197*, 109839. **DOI:**10.1016/j.dyepig.2021.109839

Povzetek

Detekcija sialne kisline v mlečnih proizvodih z naprednimi senzorji je ključna v živilski industriji. Namen predstavljenega dela je uporaba grafenskih kvantnih pik, pridobljenih iz kostne moke, dopiranih z žveplom in dušikom ter funkcionaliziranih z boronsko kislino (Boro-S/N-dGQDs) kot nanosenzorji za določanje sialne kisline. Nanodelce S/N-dGQDs smo funkcionalizirali s 4-karboksifenilboronsko kislino z namenom izboljšanja flurescenčnih lastnosti senzorja za določanje sialne kisline. Vezavo boronske kisline na površino S/N-dGQD smo potrdili z različnimi spektralnimi metodami karakterizacije. Dodatek različnih množin sialne kisline je povzročil proporcionalno korelacijo s fluorescenčnimi lastnostmi. Meritve kažejo široko linearno območje od 50 ng/mL do 1000 ng/mL in mejo določljivosti 6.04 ng/mL. Metoda izkazuje tudi dobro selektivnost, najverjetneje zaradi interakcije med 1,2-diolom sialne kisline in hidroksilno skupino Boro-S/N-dGQDs nanosenzorja. Pripravljeni senzor kaže dobro stabilnost in ponovljivost. Analize sialne kisline v različnih mlečnih proizvodih v realnem času potrjujejo uporabnost senzorjev na osnovi Boro-S/N-dGQDs.



Except when otherwise noted, articles in this journal are published under the terms and conditions of the Creative Commons Attribution 4.0 International License